Journal of Alloys and Compounds 1001 (2024) 175101

Contents lists available at ScienceDirect

Journal of Alloys and Compounds

journal homepage: www.elsevier.com/locate/jalcom

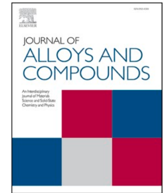

Understanding interfacial compounds induced by Ag diffusion on improving interface electrical contact resistivity between the Cu electrode and Bi_2Te_3 thin film

Zeyu Liu [a], Limei Shen [a,b,*], Junhao Yan [a], Zun Liu [a], Zhichun Liu [a,**]

[a] School of Energy and Power Engineering, Huazhong University of Science and Technology, Wuhan 430070, China
[b] Shenzhen Huazhong University of Science and Technology Research Institute, Shenzhen 518057, China

ARTICLE INFO

Keywords:
Electrical contact resistance
Interfacial compounds
Element diffusion
Electrical contact measurement
Thermoelectric thin film

ABSTRACT

It has been reported that introducing Ag interlayer at the Cu/Bi_2Te_3 interface can achieve ultra-low electrical contact resistivity. However, there is no consensus on the influence of Ag diffusion induced by Ag interlayer on electrical contact. Thus, the impact of Ag diffusion on electrical contact conductivity for Cu/Ag/Bi_2Te_3 multilayers was investigated. The generation of interfacial compounds induced by Ag diffusion was analyzed and the contact resistivity was measured in Cu/Ag/Bi_2Te_3 multilayers with different Ag interlayer thickness before and after annealing. It was found that Ag diffusion induced interfacial compounds $Cu_4Ag_3Te_4$ at the Cu/Ag interface before annealing, which could decrease contact resistivity to 3.728×10^{-12} Ω•m^2. After annealing, the relative amount of $Cu_4Ag_3Te_4$ at the Cu/Ag interface slightly decreased, and the Ag_2Te was found to appear at the Ag/Bi_2Te_3 interface, which could further decrease contact resistivity to 3.187×10^{-12} Ω•m^2. With Ag interlayer thickness increasing from 50 nm to 300 nm, the contact resistivity decreased from 3.726×10^{-10} Ω•m^2 to 3.728×10^{-12} Ω•m^2 before annealing because the relative amount of $Cu_4Ag_3Te_4$ increased about 5 times, after annealing the contact resistivity further decreased by 10.27~41.7 % because the relative amount of Ag_2Te increased about 1.1 times. In addition, we had optimized the ultra-low contact resistivity test method by redesigning the structure of test samples and modifying the formula of contact resistivity to eliminate two errors. One is caused by Cu electrode short-circuit resistance due to the test current being short-circuited by the middle electrode between two test electrodes. The other is caused by the increased electrical resistance of Bi_2Te_3 thin film due to Te atom volatilization after annealing. The results showed that the errors of the test results were reduced by at least 21.50 %. Our work provides guidance for further optimizing electrical contact of thin-film thermoelectric devices.

1. Introduction

Thin film thermoelectric coolers (TFTECs) are developing rapidly over the past two decades, which are believed as one promising method for thermal management of microchip hotspots due to its high cooling flux [1]. The maximum cooling flux $q_{c,max}$ of a TFTEC can be calculated as Eq. (1) [2]

$$q_{c,\max} = \frac{\alpha^2 T_c^2}{2\rho l} \tag{1}$$

where α, ρ and k are respectively the Seebeck coefficient, the electrical resistivity and the thermal conductivity of the thermoelectric material, l is the height of thermoelectric leg, and T denotes the temperature. It can be seen in the Eq. (1) that TFTECs have the potential to achieve high cooling flux owing to its low thermoelectric leg height. However, the reported TFTEC prototypes barely can achieve such high cooling flux. For instance, Bulman et al.[3] presented a TFTEC, which was fabricated using thin (8.1 μm) Bi_2Te_3-based thin-film superlattice materials with high intrinsic ZT of 1.5 at 303 K. According to Eq. (1) and the properties of the superlattice materials, the TFTEC can achieve a theoretic maximum cooling flux of 3080 W/cm^2. But the actual experiment result was only 258 W/cm^2. This is because the contact resistance R_c at the

* Corresponding author at: School of Energy and Power Engineering, Huazhong University of Science and Technology, Wuhan 430070, China
** Corresponding author.
E-mail addresses: EP_Shenlimei@hust.edu.cn (L. Shen), zcliu@hust.edu.cn (Z. Liu).

https://doi.org/10.1016/j.jallcom.2024.175101
Received 4 March 2024; Received in revised form 21 May 2024; Accepted 5 June 2024
Available online 6 June 2024
0925-8388/© 2024 Elsevier B.V. All rights reserved, including those for text and data mining, AI training, and similar technologies.

electrode/TE leg interface greatly degrades its cooling ability [4,5]. Considering the influence of the electrical contact resistance R_c, the actual maximum cooling flux $q_{c,max}$ should be expressed as

$$q_{c,\max} = \frac{\alpha^2 T_c^2}{2\rho l + 4R_c S} \quad (2)$$

where S is the cross-section area of thermoelectric leg. From Eq. (2), It can be seen that the contact resistance R_c significantly degrades $q_{c,max}$ due to the low l of TFTEC (<100 μm). Therefore, it's necessary to optimize the electrical contact at the electrode/TE leg interface of TFTEC [5].

To date, many methods for optimizing the electrical contact at the electrode/TE leg interfaces have been studied, most of which can be concluded into metallization and interlayers design, interface treatment, and heavy doping technique or the combination of them [6–9]. And inserting interlayers is always the first-choice method because it can not only control the electrical contact resistance but also enhance the bonding strength and interface stability [10,11]. Ni was the first kind of interlayer to be introduced to optimize the electrical contact between copper and Bi_2Te_3, which was proposed by Mengali and Selier in 1962 and decreased the electrical contact resistivity ρ_c to ~10^{-10} Ω•m^2 in macro-TEC [12]. Nowadays, Ni is still the most common interlayer for commercial TECs. However, it had been observed that Ni rapidly diffused several microns into the Bi_2Te_3, formed a NiTe phase and degraded its performance, indicating that Ni may not be the suitable interlayer for TFTEC [13,14]. Hence, researchers selected Co, Mo, Sb, Ti, etc. as interlayers and evaluated their electrical contact properties, trying to identify the optimal interlayer, as shown in Fig. 1[3,11,12, 15–20]. Fig. 2 summarize the electrical contact resistivity ρ_c of these interlayers, in which the ρ_c of most interlayers were reported in the range of 10^{-8}~10^{-10} Ω•m^2. But it's generally considered that the effect of interfacial contact resistance on TFTEC can only be neglected when the contact resistivity decreases to ~10^{-11} Ω•m^2[21]. Creating such low contact resistivities is challenging from a fabrication perspective [22], and only Co [16], Cr, Ag [20] interlayers can keep the electrical contact

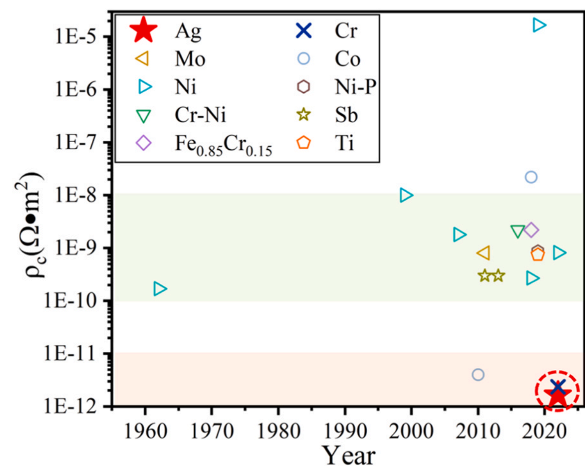

Fig. 2. Summary of interlayer materials and corresponding contact resistivities for Bi_2Te_3-based thermoelectric materials [3,11,12,16–20,25–30].

resistivity below 10^{-11} Ω•m^2 For Co interlayer, the reduction in contact resistivity is attributed to the electrically favorable interfacial phase formation [16]. For Cr interlayer, the reduction in contact resistivity is attributed to the lower potential barrier height and blocking Cu diffusion after introducing Cr [20]. For Ag interlayer, the reduction in contact resistivity is mainly attributed to the lower potential barrier height after introducing Ag interlayer. However, it's worth noting that Ag diffusion after annealing furtherly decreases the electrical contact resistance by 43.08 % [20]. While this conclusion of Ag diffusion optimizing the electrical contact conflicts earlier findings. For instance, Wu et al.[23] found that Ag diffusion may lead to a slight Seebeck-power drop in TEGs, which indicated Ag diffusion may degrade the electrical contact. Lin et al.[24] observed severe inter-diffusion between Ag interlayer and Bi_2Te_3 and an Ag_2Te compound layer was formed. The Ag_2Te compound layer had some voids and partly broke off from the Bi_2Te_3 leg, which was

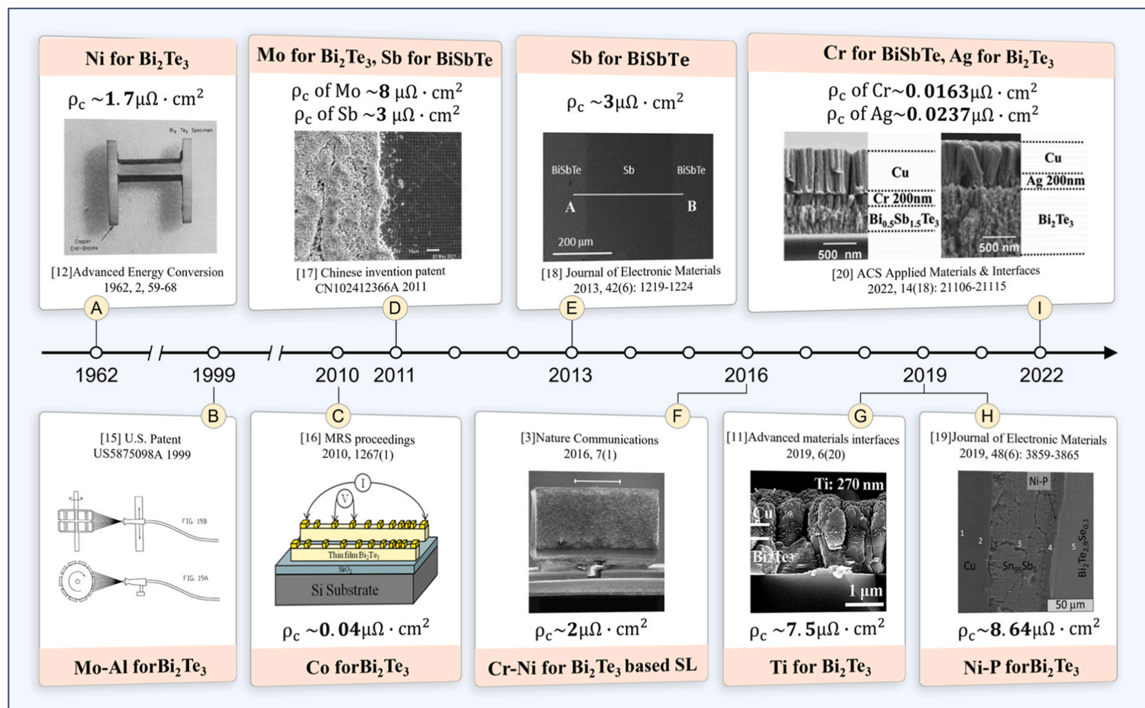

Fig. 1. The development of interlayer materials for Bi_2Te_3-based thermoelectric materials[3,11,12,15–20]. Reproduced with permission from Ref.[3,11,16,18–20]. Copyright 2016 Springer Nature. Copyright 2019 John Wiley and Sons. Copyright 1962 Elsevier. Copyright 2010 Springer Nature. Copyright 2013 Springer Nature. Copyright 2019 Springer Nature. Copyright 2022 American Chemical Society.

likely to significantly increase the electrical contact resistance. In view of the conflicts, it is meaningful to find out the principle of Ag diffusion affecting electrical contact, which may be helpful to achieve lower contact resistivities.

To find out the principle, we review previous researches about interlayer diffusion affecting electrical contact. And we consider that interfacial compounds generating by Ag interlayer diffusion may be responsible for the conflicts because similar phenomena have been observed in previous researches [16,31–36]. For instance, Shen et al. [33] reported an Ohmic contact for the junction of p-type $Nb_{0.8}Ti_{0.2}FeSb$ and Mo electrode with a low contact resistivity of $<10^{-10}$ $\Omega{\bullet}m^2$ due to the interfacial compounds FeMo induced by the diffusion of Fe into Mo. Zhao et al. [36] concluded that the growth of intermetallic compound layers formed between $CoSb_3$ and W–Cu electrode may result in the increase of contact resistance $CoSb_3/Ti/W_{80}Cu_{20}$ multilayer. So, we speculate that Ag interlayer diffusion may also lead to the generation of interfacial compounds and affect the contact resistivity.

To confirm the speculation, we investigate the relationship between the variation of electrical contact resistivity and the generation of interfacial compounds. Firstly, a group of $Cu/Ag/Bi_2Te_3$ multilayer film samples with Ag interlayer thickness of 300 nm are fabricated and half of them are annealed. The interfacial element diffusion and the types of interfacial compounds in the $Cu/Ag/Bi_2Te_3$ multilayer film are characterized and analyzed before and after annealing, respectively. Secondly, considering that the contact resistivity will be affected by the thickness of interlayer [11], 6 groups of multilayer film samples with different Ag interlayer thickness are fabricated. The relative amount of interfacial compounds and the electrical contact resistivity under different Ag interlayer thickness are measured and analyzed. Moreover, in view of measurement errors caused by the short-circuit resistance of the Cu electrode and Te atom volatilization after annealing in previous work [20], we further improve the ultra-low contact resistivity measurement method.

2. Experiments and methods

2.1. Film deposition and patterning

A magnetron sputtering system (PD-500 C, Wuhan PDVACUUM Technologies Co., Ltd) was used to deposit the $Cu/Ag/Bi_2Te_3$ multilayer thin films. Polished aluminium oxide wafers (HeFei Crystal & Surface Technical Material Co., Ltd) were used as substrates, which were (0001) oriented and had been cleaned before sputtering. To pattern the film, two kinds of masks were fixed on the substrate via an alignment device. The Bi_2Te_3 thin film was firstly deposited, followed by Ag films with different thickness, and finally the Cu film was deposited. The patterned Cu thin films can be used as electrodes for measuring the contact resistivity. The full process was shown in the Fig. 3. It can be seen that ten Cu electrodes had been deposited on the substrate. And the distances between them were respectively 0.5 mm, 1 mm, 1.5 mm, 2 mm, 2.5 mm, 3 mm and 3.5 mm, which was intentionally designed for electrical contact measurement.

The 4-inches diameter hot-press Cu (99.995 % purity), Ag (99.99 % purity) and Bi_2Te_3 (99.99 %) targets (purchased from ZhongNuo Advanced Material (Beijing) Technology Co., Ltd) were used for thin film deposition. The sputtering modes for different targets were all DC power. The sputtering power for Bi_2Te_3, Cu and Ag targets were 60 W, 80 W and 60 W respectively. The substrate was heated and maintained at 373 K. The whole deposition process was conducted in an Ar atmosphere of 1.2 Pa.

In order to investigate the generation of interfacial compounds and the contact resistivity under different Ag interlayer thickness, six groups of $Cu/Ag/Bi_2Te_3$ multilayer thin film samples were prepared. The thickness of Cu and Bi_2Te_3 layers were 1 μm and 1.5 μm respectively. The thickness of Ag interlayer was adjusted to 50 nm, 100 nm, 150 nm, 200 nm, 250 nm and 300 nm by controlling the sputtering time. However, for X-ray photoelectron spectroscopy (XPS) combined with argon ion depth etching, the thickness of Cu, Ag and Bi_2Te_3 layers were specially set as 20 nm, in order to reduce the time of argon ion depth etching.

Additionally, to investigate the generation of interfacial compounds and the contact resistivity under different Ag interlayer thickness before and after annealing, some samples were subjected to constant temperature annealing heat treatment. The annealing temperature was 473 K, the atmosphere was N_2 and the duration time was 1 hour.

2.2. Film measurement and characterization

The cross-plane microstructure and element diffusion of multilayer thin films were observed by scanning electron microscopy (SEM, Zeiss sigma300, Zeiss Geminisem 300, Hitachi SU8230) and energy-dispersive X-ray spectroscopy (EDS, Oxford X-MAX). The compounds compositions in the multilayer thin films were detected via X-ray diffraction (XRD, x'pert pro MPD, PANalytical B.V.). And the element distribution with depth was analyzed by X-ray photoelectron spectroscopy (XPS, AXIS-ULTRA DLD-600 W, KRATOS Hokkaido Co., Ltd.).

In addition, thermoelectric properties of the deposited Bi_2Te_3 thin film were examined. The carrier type and concentration of Bi_2Te_3 thin film was measured before and after annealing respectively using HET-3RT Hall effect test system (Joule Yacht, China). The Seebeck coefficient and electrical conductivity were measured by the MRS (Joule Yacht, China) thermoelectric thin film parameter testing system; And the thermal conductivity was measured via the 3ω method using TCT-HT thin film thermal conductivity test system (Joule Yacht, China) [37]. The results are shown in the Supporting Data 1.1 and 1.2.

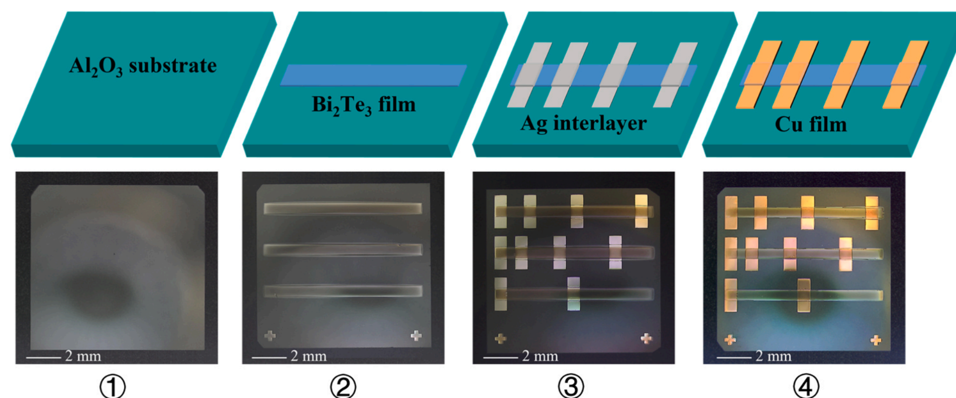

Fig. 3. Process of film deposition and patterning.

2.3. Electrical contact measurement

The electrical contact properties were measured by four-probe method and modified four-probe transmission line matrix (TLM) method. The experiment setup is shown in Supporting data 1.3. Firstly, the contact resistance R_c of $Cu/Ag/Bi_2Te_3$ was tested by the four-probe method. Secondly, the contact resistivity ρ_c of the multilayer film was further measured in combination with the modified TLM method. Compared to the unmodified TLM method in previous study [20], the modified TLM method eliminates the errors caused by Cu electrode short-circuit resistance and increased electrical resistance of annealed Bi_2Te_3 thin film via redesigning the structure of the tested samples and optimizing the calculation formula. The modified method results in a reduction of errors at least 21.50 % in comparison with unmodified method, and the comparison of all results is shown in the Supporting Data 1.4.

The principle of four-probe method is shown in Fig. 4. Fig. 4(a) shows the schematic of sample for the four-probe method. Four probes were connected in pairs to the voltmeter and ammeter respectively, and were finally connected to point 1, 2, 3, and 4. During the test, current flowed in and out through probe 1 and probe 2. The test current passes by the sample ranged from −6 mA to 6 mA in steps of 1 mA, and the positive value refers to inflow from Probe 1 and outflow from Probe 2. Fig. 4(b) shows the according resistance network diagram.

R_s is the electrical resistance of Bi_2Te_3 thin films between probes. R_t is the resistance of the probe joint. R_d is the resistance of Cu electrode. The numbers in the superscripts represents the corresponding probe positions, e.g., R_{d1} represents the resistance of Cu electrode through which current flows at probe 1, and R_{s12} represents the sheet resistance of Bi_2Te_3 thin films between probe 1 and probe 2.

The voltmeter measurement is U_c and the ammeter measurement is I. So, the contact resistance R_c can be calculated:

$$R_c = U_c / I \tag{3}$$

The principle of the unmodified TLM method is shown in Fig. 5. Fig. 5(a) shows the schematic of test sample for the unmodified TLM method with equidistant electrodes, the distance between electrodes is d. Electrode ① and ②, ① and ③, ① and ④ are sequentially used as the test electrodes. In the test, the probe is connected to two test electrodes, ammeter, voltmeter, and DC power supply. Current flows in from one test electrode and out from the other. The magnitude of this current is measured using an ammeter and the voltage between the two test electrodes is measured using a voltmeter. Here, the test current is kept at 1 mA by adjusting the DC power supply. R_T denotes the measurement result of total electrical resistance, which is obtained via dividing the voltmeter measurement by the ammeter measurement. D is the length of the exposed Bi_2Te_3 thin film between the test electrodes. Hence, a graph of R_T versus D can be made, as shown in the Fig. 5(b). The details of the unmodified TLM method have been described in our previous work [20]. The errors of the unmodified TLM method are twofold. On the one hand, the measurement results of ρ_c were affected by the short-circuit resistance of Cu electrode due to the electrode arrangement. As shown in the Fig. 5(c)(d), the current would be short-circuited by the middle electrode when flowing through it, resulting in additional R_c and R_d, which made the measured ρ_c larger than the true value. On the other hand, the measurement results of ρ_c were affected by the Te atoms volatilization after annealing. The Te atoms in the Bi_2Te_3 thin film volatilized after annealing, which led to tellurium vacancies ($V_{Te}^{\cdot\cdot}$). And the $V_{Te}^{\cdot\cdot}$ could be occupied by neighboring Bi atoms, which led to a pair of bismuth vacancy (V_{Bi}) and antisite defect $Bi_{Te}^{\cdot}$. This series of crystal defects resulted in an increase in the resistance of n-type Bi_2Te_3 thin film [38] and affected the measurement which made the measured ρ_c lower than the true value.

Therefore, we modified the TLM method from the previous work [20] to eliminate the errors caused by the short-circuit resistance of the Cu electrode and the increase in resistance of annealed Bi_2Te_3 thin film.

First, the electrode spacing was redesigned to be an arithmetic progression in order to eliminate the errors caused by the short-circuit resistance of the Cu electrode as shown in the Fig. 6(a). Electrode ① and ②, ② and ③, ③ and ④ were sequentially used as the test electrodes. The graph of R_T versus D is shown in the Fig. 6(b). The resistance network diagram during the test is shown in the Fig. 6(c), and the current flow inside the modified sample is shown in the Fig. 6(d). It can be seen that there were no middle electrodes between the test electrodes, so the errors caused by the short-circuit resistance of the Cu electrodes can be eliminated.

Second, the calculation formula of ρ_c was optimized in order to eliminate the errors caused by the increase in the resistance of the annealed Bi_2Te_3 thin film. The optimization is based on the assumption in TLM method. TLM method assumes that the contact resistance R_c, the sheet resistance of Bi_2Te_3 thin film in the contact region R_{sk}, and the width of the thin film in the contact region w had the following relationship

$$R_c = R_{sk} \bullet L_T / w \tag{4}$$

L_T was the transmission length. And it was assumed that

$$R_{sk} = R_{sh} \tag{5}$$

R_{sh} was the sheet resistance of Bi_2Te_3 thin film between electrodes. Because the contact resistivity ρ_c can calculated by $\rho_c = R_c \bullet w \bullet L_T$, it can be transformed into Eq. (6) in combination with Eq. (4)(5).

$$\rho_c = R_c{}^2 \bullet w^2 / R_{sh} \tag{6}$$

The calculation result of Eq. (4) is correct for the as-deposited samples but wrong for the annealed samples. Because the sheet resistance R_{sh} of annealed Bi_2Te_3 thin film was larger than that of as-deposited Bi_2Te_3 thin film, i.e., $R_{sh,an} > R_{sh,as}$. And the multilayer structure can effectively hinder the volatilization of Te atoms in the contact region [39]. Therefore, the original assumption that $R_{sk} = R_{sh,an}$ was no longer

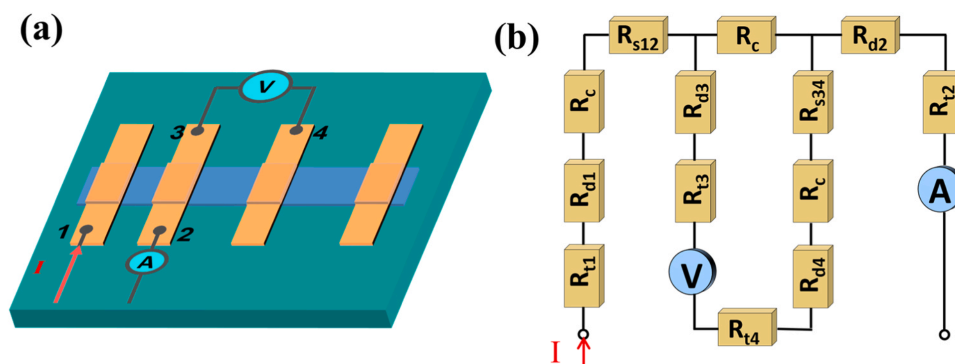

Fig. 4. Principle of four-probe method. (a) schematic of sample for the four-probe method. 1–4 is the position of probes; (b) resistance network diagram.

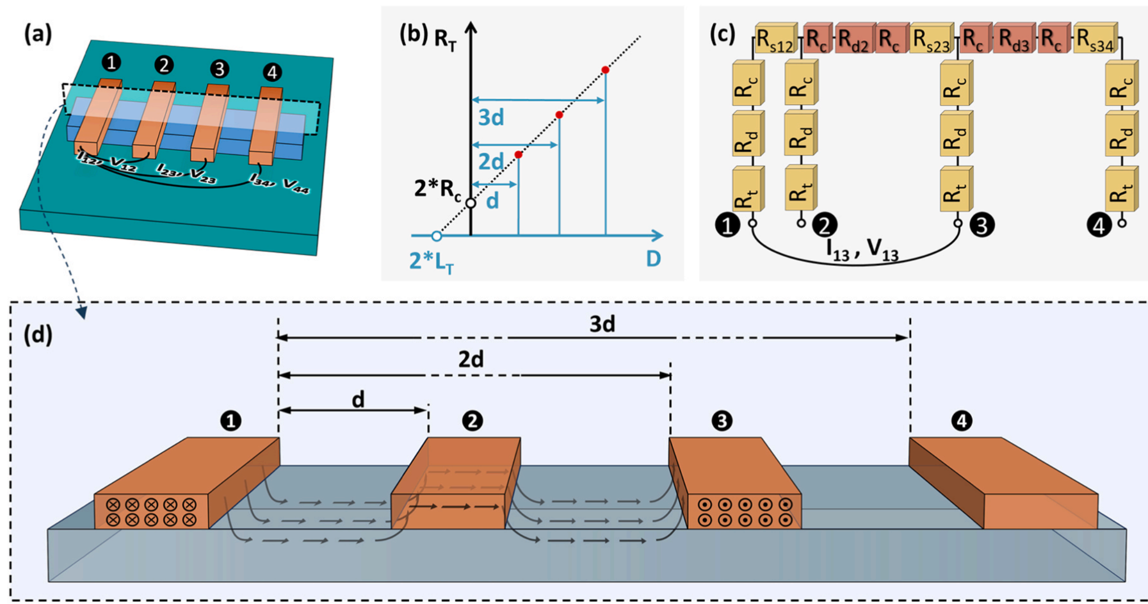

Fig. 5. Principle of unmodified TLM method. (a) schematic of test sample for the unmodified TLM method with equidistant electrodes; (b) diagram of the total resistance R_T vs distance d between probes; (c) electrical resistance network diagram; (d) schematic of current flow in the sample.

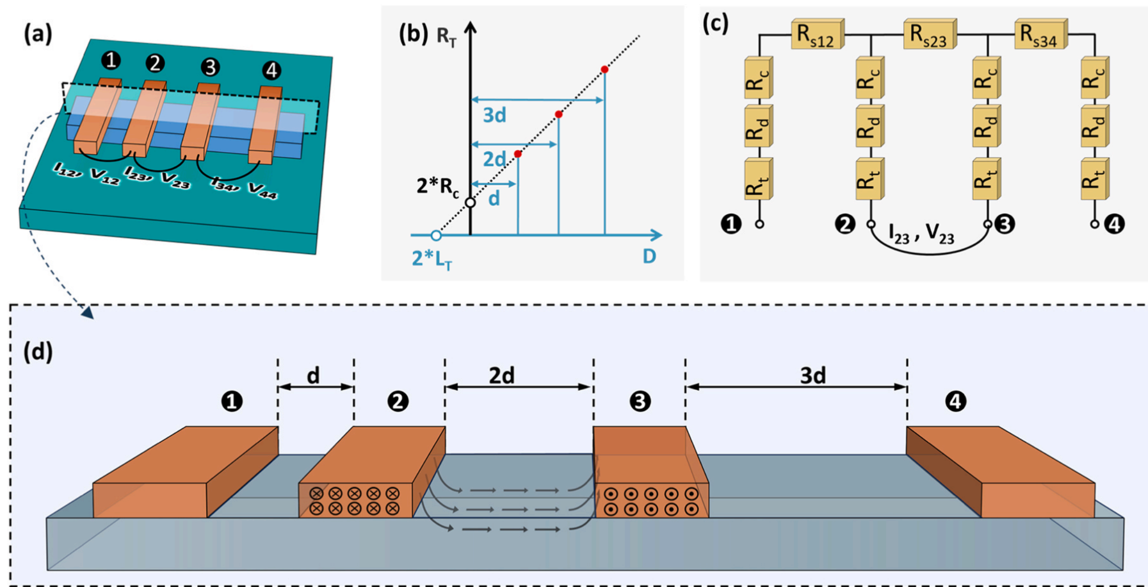

Fig. 6. Principle of modified TLM method. (a)schematic of test sample for the modified TLM method; (b) diagram of the total resistance R_T vs distance d between probes; (c) electrical resistance network diagram; (d) schematic of current flow in the modified sample.

valid for the annealed samples. To eliminate the errors, it was supposed to assume that R_{sk}=$R_{sh,as}$. So, the contact resistivity of annealed samples $\rho_{c,an}$ should be calculated as below:

$$\rho_{c,an} = R_{c,an}{}^2 \bullet w^2 / R_{sh,as} \quad (7)$$

And the contact resistivity of as-deposited samples $\rho_{c,as}$ should be calculated as below:

$$\rho_{c,as} = R_{c,as}{}^2 \bullet w^2 / R_{sh,as} \quad (8)$$

3. Results and discussions

3.1. Analysis of interfacial compounds types

Firstly, the micro-structure of Bi_2Te_3 was characterized by SEM and XRD. The SEM image of as-deposited Bi_2Te_3 thin film in cross-plane direction is shown in the Fig. 7(a). And XRD result is shown in the Fig. 7(d). It can be seen that diffraction peaks are intense and sharp, indicating that the as-deposited Bi_2Te_3 thin film has a high degree of crystallinity and exhibits highly preferential orientation along the (0 1 5) plane (PDF#15–0863). Then Bi_2Te_3 thin film was annealed with the heat-treatment conditions as described in Section 2.1. The SEM image of the annealed Bi_2Te_3 thin film in the cross-plane direction is shown in the Fig. 7(e), and the XRD results is shown in the Fig. 7(h). Compared with Fig. 7(d), a new sharp diffraction peak with an orientation of (1 0 10) appears in the XRD pattern (PDF#15–0863). It indicates that recrystallization occurred in the Bi_2Te_3 thin film during annealing and partly changed the orientation.

SEM and XRD were also performed on as-deposited $Cu/Ag/Bi_2Te_3$ multilayer film with Ag interlayer thickness of 300 nm. Fig. 7(b) is the

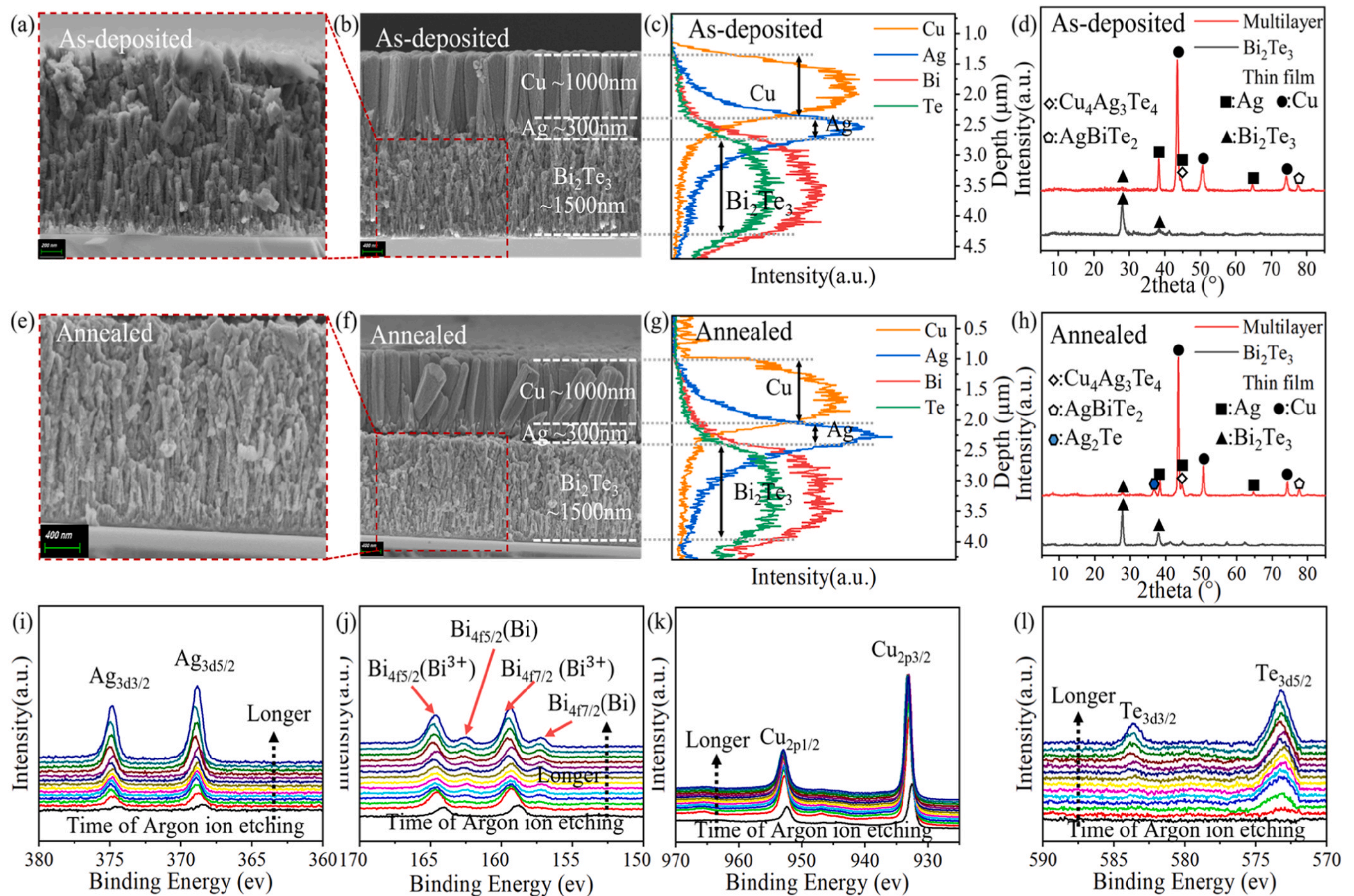

Fig. 7. Analysis of interfacial compounds types. (a) SEM of as-deposited Bi_2Te_3 thin film and (b) as-deposited Cu/Ag/Bi_2Te_3 multilayer thin film; (c) EDS line profile depths of as-deposited Cu/Ag/Bi_2Te_3 multilayer thin film; (d) XRD of annealed Bi_2Te_3 and Cu/Ag/Bi_2Te_3 multilayer thin film; (e) SEM of annealed Bi_2Te_3 thin film and (f) annealed Cu/Ag/Bi_2Te_3 multilayer thin film; (g) EDS line profile depths of annealed Cu/Ag/Bi_2Te_3 multilayer thin film; (h) XRD of annealed Bi_2Te_3 and Cu/Ag/Bi_2Te_3 multilayer thin film; XPS analysis results of (i) Ag (j) Bi (k) Cu and (l) Te in annealed Cu/Ag/Bi_2Te_3 multilayer thin film.

SEM image in the cross-plane direction, and Fig. 7(c) is the EDS line scan results. Although the interface of the Cu/Ag/Bi_2Te_3 film is clear in the SEM image, the EDS line profile depths demonstrated that the Cu, Ag, Bi, and Te elements all slightly diffused near the interface. To determine the generation of interfacial compounds, XRD tests were performed on the multilayer film and the results are shown in the Fig. 7(d). It can be seen that the XRD pattern includes other compounds besides Cu, Ag and Bi_2Te_3. Combined with the EDS line profile depths, the diffraction peak at 2θ=77.52° represents the (1 0 16)-oriented $AgBiTe_2$ (PDF#18–1173), which was generated near the Ag/Bi_2Te_3 interface. Because it is likely to combine with Ag elements to generate Ag-Bi-Te interfacial compound due to the high content of Bi and Te elements near the Ag/Bi_2Te_3 interface. The diffraction peak at 2θ=44.25° includes the (6 0 0)-oriented $Cu_4Ag_3Te_4$ (PDF#18–1173) and the (2 0 0)-oriented Ag. The $Cu_4Ag_3Te_4$ was generated near the Cu/Ag interface. Because the Ag layer near the Cu/Ag interface has a high content of Cu, Ag, and Te elements, there is a high probability that they combine with each other to generate Cu-Ag-Te interfacial compounds. Meanwhile, according to the SEM image of Fig. 7(b), the Cu and Ag grains were tightly bonded and had similar crystal orientations. Moreover, it can be determined in the XRD pattern that the diffraction peaks at 2θ=43.47°,50.60° and 74.30° represents the (1 1 1 1), (2 0 0) and (2 2 0) orientations of Cu respectively, and the diffraction peaks at 2θ=37.93° and 64.66° represents the (1 1 1 1) and (2 2 0) orientations of Ag, respectively. So, the (2 0 0) orientation of Ag should also exist.

The annealed Cu/Ag/Bi_2Te_3 multilayer film with Ag interlayer thickness of 300 nm was measured with SEM, EDS and XRD, too. The results are shown as Fig. 7(f)(g)(h) respectively. Obviously, although the SEM and EDS results of as-deposited and annealed multilayer thin film are similar, the XRD pattern reveals that (2 1 1)-oriented Ag_2Te (PDF#42–1266) interfacial compounds appeared in the multifilm after annealing. Li et al. [24] annealed Ag/Bi_2Te_3 bilayer films at 250 °C and detected the generation of Ag_2Te at the interface between Ag and Bi_2Te_3. The Ag_2Te generated after annealing in the present study may be similar to this, which was also generated at the Ag/Bi_2Te_3 interface. Notably, the Cu (1 1 1) diffraction peak is too sharp and intense, which makes the other peaks difficult to be recognized in the XRD patterns. Thus, the following XRD patterns would be processed and the Cu (1 1 1) diffraction peak would be removed to facilitate the observation of the other diffraction peaks.

X-ray photoelectron spectroscopy (XPS) combined with argon ion depth etching was used to obtain more detailed information about the chemical and bonding environment around the Ag interlayer. Samples were fabricated and annealed under the same operating parameters in Section 2, the thickness Cu, Ag and Bi_2Te_3 layers were adjusted to 40 nm, 20 nm and 20 nm, respectively. The test results were corrected using the $C_{1\ s}$ peak value of 284.8 eV, as shown in Fig. 7(i)(j)(k)(l). The different curves correspond to different etching times. The longer the etching time is, the deeper the depth is, and the maximum depth is reached when the etching time reaches 6100 s.

The peaks at ~368.85 eV and ~374.95 eV correspond to $Ag_{3d5/2}$ and $Ag_{3d3/2}$ in Fig. 7(i), which means the presence of Ag^+. And peaks at ~159.3 eV and ~164.6 eV correspond to $Bi_{4f7/2}$ and $Bi_{4f5/2}$ in Fig. 7(j), which means the existence of Bi^{3+}. With the increase of argon ion

etching time and the deeper XPS detection depth, the weak peaks at ~157.15 eV and ~ 162.5 eV gradually appears, which represent Bi metal. The reason for the existence of Bi metal may be that the Cu and Ag layers was too thin to prevent Te atoms from diffusing to the top of multilayer film and then volatilizing. So, there was a lack of Te atoms at the bottom of multilayer film, resulting in a small number of Bi atoms losing coordination and becoming Bi metal. The peaks at ~933.15 eV and ~952.85 eV correspond to $Cu_{2p3/2}$ and $Cu_{2p1/2}$ in Fig. 7(k), which indicates the presence of Cu^{+} and Cu^{2+}[40]. And the peaks at ~573.10 eV and ~583.65 eV correspond to $Te_{3d5/2}$ and $Te_{3d3/2}$ in the Fig. 7(l), indicating the presenceTe^{2-}. So, the XPS analysis results accorded with the XRD test results. Additionally, in order to investigate the stability of those interfacial compounds, we aged a set of samples at room temperature for 20 months and re-test them. The results showed that $Cu_4Ag_3Te_4$ and Ag_2Te can still be detected, which had great stability. However, $AgBiTe_2$ can't be detected anymore, which may indicate that $AgBiTe_2$ is less stable under room temperature. The detailed results of XRD and electrical contact measurement are shown in Supporting Data 1.5.

In summary, there were two types of interfacial compounds, $AgBiTe_2$ and $Cu_4Ag_3Te_4$ in the as-deposited Cu/Ag/ Bi_2Te_3 multilayer thin film. $AgBiTe_2$ was generated at the Ag/Bi_2Te_3 interface. $Cu_4Ag_3Te_4$ was generated at the Cu/Ag interface. After annealing, the third type of interfacial compound Ag_2Te appeared, which was generated at the Ag/Bi_2Te_3 interface.

3.2. Variation with thickness

Considering that the contact resistivity will be affected by the thickness of interlayer [11], six groups of multilayer thin film samples with Ag thicknesses of 50 nm, 100 nm, 150 nm, 200 nm, 250 nm, and 300 nm were prepared and tested respectively. The results of the measurements are shown in Fig. 8.

The as-deposited multilayer thin films with different Ag thicknesses were firstly tested by the four-probe method, and the V-I test results are shown in Fig. 8(a). The measurements of the six groups shows good linearity, and all the curves intersects at (0,0), which indicates that they are all ohmic contacts. Based on the V-I curve measurements, the contact resistance $R_{c,as}$ was further analyzed to obtain the variation of contact resistance $R_{c,as}$ with Ag thickness, as shown in Fig. 8(b). The contact resistance $R_{c,as}$ monotonically decreases with increasing Ag thickness. Compared with the $R_{c,as}$ of 0.308 Ω for the sample with Ag thickness of 50 nm, the $R_{c,as}$ for the sample with Ag thickness of 300 nm is only 0.035 Ω, which decreases by 88.78 %. Then, the sheet resistance $R_{sh,as}$ of the as-deposited Bi_2Te_3 film and contact resistivity $\rho_{c,as}$ of as-deposited multilayer film was measured in sequence by the modified TLM method. The diagram of $R_{sh,as}$ vs Ag thickness is shown in Fig. 8(c). It can be seen that the variation is not obvious, which is in the range of 100 Ω ~ 117 Ω. Measurement results of $\rho_{c,as}$ were shown in Fig. 8(d). The results illustrate that $\rho_{c,as}$ decreases exponentially with increasing Ag thickness. As the Ag thickness increases from 50 nm to 300 nm, the $\rho_{c,as}$ decreases from 3.276×10^{-10} Ω•m^2 to 3.728×10^{-12} Ω•m^2, which is slightly better than that in our previous study [20].

In order to investigate the relationship between contact properties and interfacial compounds, XRD was used to analyze the as-deposited Cu/Ag/Bi_2Te_3 multilayer thin film samples with Ag thicknesses from 50 to 300 nm. The XRD results are shown in Fig. 8(e), which had been processed as illustrated in Section 3.1. The complete original XRD patterns are shown in Supporting Data 1.6. Semi-quantitative analysis was carried out using the RIR value method to calculate the relative amount of the interfacial compounds within the different samples, and the results are shown in Fig. 8(f). The details of RIR value method are also shown in Supporting Data 1.6. As shown in Fig. 8(f) the relative amount of $Cu_4Ag_3Te_4$ is significantly higher than that of $AgBiTe_2$ in the as-deposited samples. And the relative amount of $Cu_4Ag_3Te_4$ increases with the increase of Ag thickness. It's because of the increasing Ag content in the multilayer film. When the Ag thickness is in the range of 50–200 nm, there is no obvious diffraction peak corresponding to $AgBiTe_2$ in the pattern. This may be because the Ag content in the multilayer film was insufficient and little $AgBiTe_2$ was generated. When

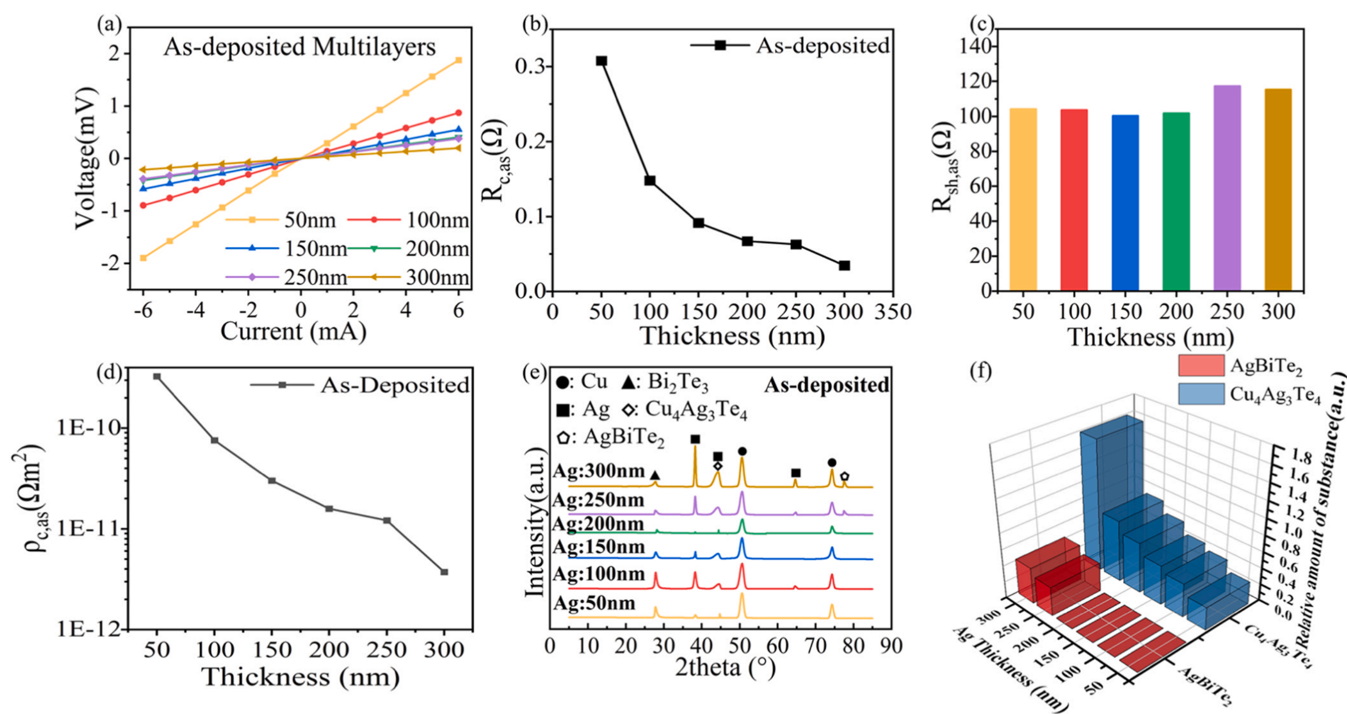

Fig. 8. Test results of as-deposited multilayer films with different Ag thicknesses. (a) I–V characteristics tested by four-probe method; (b) Variation of contact resistance $R_{c,as}$ with Ag thickness; (c) Variation of Bi_2Te_3 film sheet resistance $R_{sh,as}$ with Ag thickness; (d) Variation of contact resistivity $\rho_{c,as}$ with Ag thickness; (e) XRD patterns of as-deposited Cu/Ag/Bi_2Te_3 multilayer films; (f) Variation of relative content of interfacial compounds with Ag thickness.

the Ag thickness increases to 250 and 300 nm, the Ag content increases, so more $AgBiTe_2$ was generated, and the diffraction signal became intense.

Based on Fig. 8(d)(f), it's speculated that the optimization of the interfacial contact properties before annealing is related to the generation of the interfacial compound $Cu_4Ag_3Te_4$. Although there is a lack of studies on the thermoelectric properties of $Cu_4Ag_3Te_4$, it has a similar elemental composition to Cu_7Te_4. Cu_7Te_4 has been proven to be a highly simplified semiconductor with a barrier height of 1.4 meV, and 3 % Ag-doped Cu_7Te_4 has a barrier height of 4.1 meV [41]. The barrier height is much lower than contact potential of the Cu/Ag interface, which is 390 meV. So, it's presumed that the barrier between Cu/ $Cu_4Ag_3Te_4$ is lower than 390 meV, and $Cu_4Ag_3Te_4$ plays an optimizing role for the Cu/Ag interface contact. $Cu_4Ag_3Te_4$ may be dispersed in the form of particles near the Cu/Ag interface and formed microcontacts. With the increase of Ag layer thickness, the $Cu_4Ag_3Te_4$ generates more, and the $Cu/Cu_4Ag_3Te_4$ microcontacts increases, which leads to further decrease of contact resistance. When the Ag thickness increases to 300 nm, the distribution of $Cu_4Ag_3Te_4$ near the Cu/Ag interface is close to saturation, so the decreasing trend of contact resistance slows down.

In summary, with the Ag interlayer thickness increasing from 50 nm to 300 nm, $\rho_{c,as}$ decreases from 3.276×10^{-10} $\Omega\bullet m^2$ to 3.728×10^{-12} $\Omega\bullet m^2$, which were all ohmic contacts. The relative amount of interfacial compounds $AgBiTe_2$ and $Cu_4Ag_3Te_4$ also increased while the Ag interlayer thickening. And $Cu_4Ag_3Te_4$ can optimize the electrical contact by lowering the barrier height at Cu/Ag interface.

3.3. Annealing

In order to investigate the influence of annealing on the generation of interfacial compounds and on the contact resistivity ρ_c, the samples were annealed under the same operating parameters in Section 2. The same tests as in Section 3.2 were performed on the annealed samples, and the results are shown in Fig. 9.

The V-I test results are shown in Fig. 9(a), from which it can be seen that the multilayer films remain in good ohmic contact after annealing. The contact resistance $R_{c,as}$ was further analyzed and the results are shown as shown in Fig. 9(b). It's found that $R_{c,an}$ maintains the same trend of decreasing with the increase of Ag thickness as $R_{c,as}$ does. When the Ag thickness increases from 50 nm to 300 nm, the $R_{c,an}$ decreases from 0.292 Ω to 0.032 Ω with a decrease of 89.04 %. $R_{c,an}$ is smaller than $R_{c,as}$ at different Ag thicknesses, and the minimum is only 77.00 % of $R_{c,as}$. The sheet resistance of annealed Bi_2Te_3 thin film $R_{sh,an}$ was measured by the modified TLM method, and the results are shown in Fig. 9(c). The $R_{sh,an}$ at different Ag thicknesses increases by 27.6~57.0 % compared with $R_{sh,as}$. The reason for $R_{sh,an}>R_{sh,as}$ has been illustrated in Section 2.3. The modified method described in Section 2.3 was used to calculate the contact resistivity of annealed multilayer thin film $\rho_{c,an}$, and the results are shown in Fig. 9(d). It can be seen that $\rho_{c,an}$ also decreases with the increase of Ag thickness, and reaches the minimum value of

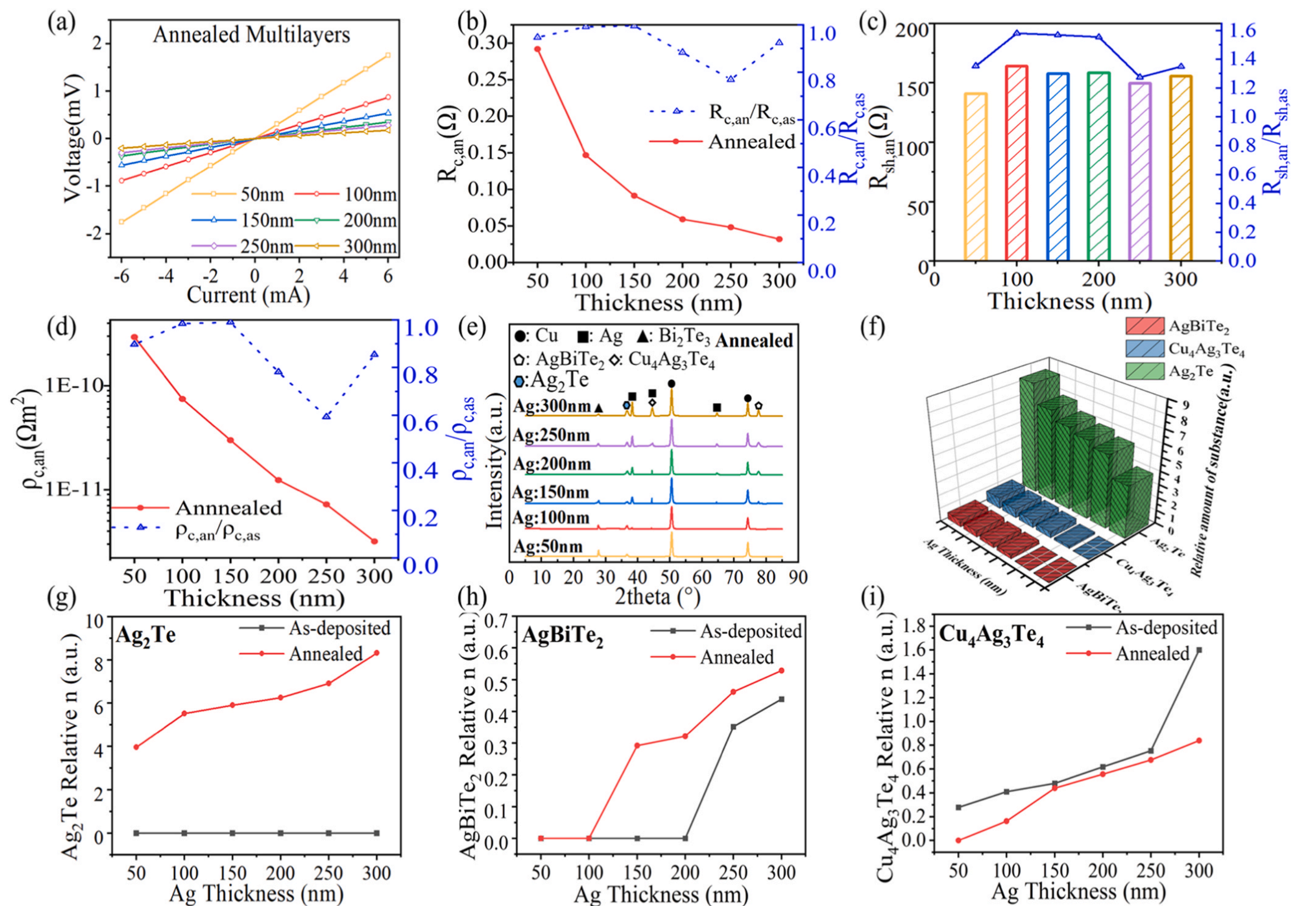

Fig. 9. Test results of annealed multilayer films with different Ag thicknesses and comparison with the results of as-deposited samples. (a) I−V characteristics tested by four-probe method; (b) Variation of contact resistance $R_{c,an}$ and $R_{c,an}/R_{c,as}$ with Ag thickness; (c) Variation of Bi_2Te_3 film sheet resistance $R_{sh,an}$ and $R_{sh,an}/R_{sh,as}$ with Ag thickness; (d) Variation of contact resistivity $\rho_{c,an}$ and $\rho_{c,an}/\rho_{c,as}$ with Ag thickness; (e) XRD patterns of annealed $Cu/Ag/Bi_2Te_3$ multilayer films; (f) Variation of relative content of interfacial compounds with Ag thickness; Variation of the relative amount of (g)Ag_2Te (h)$AgBiTe_2$ (i)$Cu_4Ag_3Te_4$ with Ag thickness before and after annealing.

3.187×10^{-12} Ω·m^2 when the Ag thickness is 300 nm. $\rho_{c,an}$ is smaller than $\rho_{c,as}$ at different Ag thicknesses, which further decreases by 10.27~41.7 % compared with $\rho_{c,as}$.

XRD was used to analyze the annealed Cu/Ag/Bi_2Te_3 multilayer thin film samples. The XRD results are shown in Fig. 9(e), which had been also processed as illustrated in Section 3.1. The complete original XRD patterns are shown in Supporting Data 1.6. Semi-quantitative analysis was performed using the RIR value method to calculate the relative amount of interfacial compounds within different samples. The results are analyzed and compared with the that of as-deposited samples, as shown in Fig. 8(f)(g)(h)(i). From the figure, it can be seen that the relative amount of Ag_2Te increases with the increase of Ag thickness. It's also due to the increasing Ag content in the multilayer film. Besides, the relative amount of the interfacial compound Ag_2Te is significantly more than that of $AgBiTe_2$ and $Cu_4Ag_3Te_4$. And the relative amount of $Cu_4Ag_3Te_4$ in annealed samples is less than that in as-deposited samples although it still increases with the increase of the Ag thickness. It may owe to the decomposition of $Cu_4Ag_3Te_4$ after annealing.

Combined with Fig. 9(d)(f)(g)(i), it's speculated that the optimization of the contact properties after annealing is related to the generation of both the interfacial compound $Cu_4Ag_3Te_4$ as well as Ag_2Te. It has been reported that the barrier height of Ag/Ag_2Te interface is 0.054 eV [42], which is lower than the 0.065 eV of Ag/Bi_2Te_3 interface [20]. Although the relative amount of $Cu_4Ag_3Te_4$ decreases slightly after annealing, a large amount of Ag_2Te is generated near the Ag/Bi_2Te_3 interface and $\rho_{c,an}$ is improved. As the thickness of the Ag layer increases, the generated Ag_2Te increases and the Ag/Ag_2Te contact increases, leading to a further decrease in $\rho_{c,an}$. When the Ag thickness increases to 300 nm, the distribution of Ag_2Te near the Ag/Bi_2Te_3 interface is close to saturation, and the decreasing trend of contact resistance slows down. Since the $Cu_4Ag_3Te_4$ decreases after annealing, and the Ag/Ag_2Te micro-contacts cannot optimize the electrical contact performance of the multilayer films as much as the Cu/$Cu_4Ag_3Te_4$ micro-contacts, the optimization of the contact resistance by heat treatment is less than that brought by the increase in thickness.

Additionally, a single-leg TFTEC model was established to compare the cooling efficiency after adding Ag layer. In the model, the electrical contact resistivity was experimental measurements and thermal contact resistivity was estimated by Wiedemann–Franz law. The results showed that the $q_{c,max}$ can achieve to 366.62 W/cm^2, and ΔT_{max} can achieve to 82.02 K after adding a 300-nm Ag layer at T_h=350 K. Details of the model are demonstrated in the Supporting Data 1.7.

Moreover, considering that the generation of Ag_2Te at the Ag/Bi_2Te_3 in bulk significantly degraded the interface reliability [24], the impact of Ag_2Te on interface bonding strength was also studied. The bonding strength of the multilayer thin film was measured before and after annealing respectively, using nano-scratch meter (Nano Indenter® G200, KLA Corporation). It was shown that bonding strength of Cu/Ag/Bi_2Te_3 multilayers barely changed before and after annealing, which was 10.39 mN and 10.44 mN respectively. The results indicated that generation of Ag_2Te in thin film didn't form structural failures and degrade the interface reliability like that in bulk. The detailed results are shown in Supporting Data 1.8.

In summary, after annealing, electrical contact resistivity further decreased by 10.27~41.7 %. and reached the minimum value of 3.187×10^{-12} Ω·m^2. Relative amount of $Cu_4Ag_3Te_4$ slightly decreased, and the Ag_2Te was found to be generated at the Ag/Bi_2Te_3 interface after annealing. The results indicated that Ag_2Te can optimize the electrical contact, which may be because Ag_2Te can lower the barrier height at Ag/Bi_2Te_3 interface. In addition, generation of Ag_2Te in thin film didn't form structural failures and degrade the interface reliability like that in bulk.

4. Conclusions

In this study, we the investigated the influence of Ag diffusion on the electrical contacts of Cu/Ag/Bi_2Te_3 multilayers and found that Ag diffusion induced interfacial compounds $Cu_4Ag_3Te_4$ and Ag_2Te, which can significantly optimize the electrical contact. The $Cu_4Ag_3Te_4$ was found to be generated at the Cu/Ag interface before annealing and its relative amount slightly decreased after annealing. The Ag_2Te was found to be generated at the Ag/Bi_2Te_3 interface after annealing. The results of electrical contact measurement demonstrated that the interfacial compounds didn't change the metal-semiconductor (M-S) contact types of the Cu/Ag/Bi_2Te_3 multilayers, which were all ohmic contacts. Overall, the contact resistivity decreases exponentially with increasing Ag layer thickness and relative amount of interfacial compounds. The relative amount of $Cu_4Ag_3Te_4$ increased ~5 times with the Ag interlayer thickness increasing from 50 nm to 300 nm before annealing, leading to the electrical contact resistivity of as-deposited multilayer $\rho_{c,as}$ decreasing from 3.276×10^{-10} Ω•m^2 to 3.728×10^{-12} Ω•m^2. The relative amount of Ag_2Te increased ~1.1 times with the Ag interlayer thickness increasing from 50 nm to 300 nm after annealing, leading to the electrical contact resistivity of annealed multilayer $\rho_{c,an}$ decreasing from 2.939×10^{-10} Ω•m^2 to 3.187×10^{-12} Ω•m^2, which were only 58.3~90.73 % of that before annealing. When Ag interlayer thickness was 300 nm, the contact resistivity tended to a constant value, which may be because the generation of $Cu_4Ag_3Te_4$ and Ag_2Te was close to saturation at the interface. The impact of Ag_2Te on the interface bonding strength was also studied. It was shown that bonding strength of Cu/Ag/Bi_2Te_3 multilayers barely changed before and after annealing, which was 10.39 mN and 10.44 mN respectively. The results indicated that generation of Ag_2Te in thin film didn't form structural failures and degrade the interface reliability like that in bulk. Additionally, the ultra-low contact resistivity test method was modified to eliminate errors caused by Cu electrode short-circuit resistance and the increased sheet resistance of Bi_2Te_3 thin film. By redesigning the structure of test samples and modifying the formula of contact resistivity, the errors of contact resistivity test results were reduced by at least 21.50 %. In conclusion, this study demonstrates that interfacial compounds induced by Ag diffusion can improve interface electrical contact resistivity between the Cu electrode and Bi_2Te_3 thin film, which provides inspiration for interface design of TFTECs.

CRediT authorship contribution statement

Zhichun Liu: Writing – review & editing, Resources, Conceptualization. **Zun Liu:** Validation, Investigation. **Junhao Yan:** Investigation, Formal analysis. **Limei Shen:** Writing – review & editing, Supervision, Resources, Funding acquisition, Conceptualization. **Zeyu Liu:** Writing – review & editing, Writing – original draft, Visualization, Validation, Methodology, Investigation, Formal analysis, Conceptualization.

Declaration of Competing Interest

The authors declare that they have no known competing financial interests or personal relationships that could have appeared to influence the work reported in this paper.

Data availability

Data will be made available on request.

Acknowledgement

This work is jointly supported by the National Natural Science Foundation of China (Grant No. 52176007), National Key Research and Development Program of China (Grant No. 2022YFB3803900), Science, Technology and Innovation Commission of Shenzhen Municipality (Grant No. JCYJ20210324115611030). And thanks engineer Liting Hu and Chenglin Shang in Optoelectronic Micro&Nano Fabrication and Characterizing Facility, Wuhan National Laboratory for Optoelectronics of Huazhong University of Science and Technology for the support in

device fabrication (stylus profiler test and wire bonding).

Appendix A. Supporting information

Supplementary data associated with this article can be found in the online version at doi:10.1016/j.jallcom.2024.175101.

References

[1] X. Shi, J. Zou, Z. Chen, Advanced thermoelectric design: from materials and structures to devices, Chem. Rev. 120 (15) (2020) 7399–7515.

[2] I. Chowdhury, R. Prasher, K. Lofgreen, G. Chrysler, et al., On-chip cooling by superlattice-based thin-film thermoelectrics, Nat. Nanotechnol. 4 (4) (2009) 235–238.

[3] G. Bulman, P. Barletta, J. Lewis, N. Baldasaro, et al., Superlattice-based thin-film thermoelectric modules with high cooling fluxes, Nat. Commun. 7 (1) (2016).

[4] R. He, G. Schierning, K. Nielsch, Thermoelectric devices: a review of devices, architectures, and contact optimization, Adv. Mater. Technol. 3 (4) (2018).

[5] L.W. Da Silva, M. Kaviany, Fabrication and measured performance of a first-generation microthermoelectric cooler, J. Micro Syst. 14 (5) (2005) 1110–1117.

[6] R. Vizel, T. Bargig, O. Beeri, Y. Gelbstein, Bonding of Bi2Te3-based thermoelectric legs to metallic contacts using Bi0.82Sb0.18 alloy, J. Electron. Mater. 45 (3) (2016) 1296–1300.

[7] S. Kim, S. Kim, G. Kim, J. Kim, et al., Ar plasma treatment for III–V semiconductor-based transistor source/drain contact resistance reduction, J. Nanosci. Nanotechnol. 16 (10) (2016) 10389–10392.

[8] P.J. Taylor, J.R. Maddux, G. Meissner, R. Venkatasubramanian, et al., Controlled improvement in specific contact resistivity for thermoelectric materials by ion implantation, Appl. Phys. Lett. 103 (4) (2013) 43902.

[9] X. Kong, W. Zhu, L. Cao, Y. Peng, et al., Controllable electrical contact resistance between Cu and oriented-Bi2Te3 film via interface tuning, Acs Appl. Mater. Interfaces 9 (30) (2017) 25606–25614.

[10] W. Wu, G. Ren, X. Chen, Y. Liu, et al., Interfacial advances yielding high efficiencies for thermoelectric devices, J. Mater. Chem. A, Mater. Renew. Sustain. Energy 9 (6) (2021) 323–329.

[11] D. Qin, W. Zhu, F. Hai, C. Wang, et al., Enhanced interface stability of multilayer Bi2Te3/Ti/Cu films after heat treatment via the insertion of a Ti layer, Adv. Mater. Interfaces 6 (20) (2019).

[12] O.J. Mengali, M.R. Seiler, Contact resistance studies on thermoelectric materials, Adv. Energy Convers. 2 (1962) 59–68.

[13] Y.C. Lan, D.Z. Wang, G. Chen, Z.F. Ren, Diffusion of nickel and tin in p-type (Bi,Sb) 2Te3 and n-type Bi2(Te,Se)3 thermoelectric materials, Appl. Phys. Lett. 92 (10) (2008) 101910.

[14] E. Yusufu, T. Sugahara, M. Okajima, S. Nambu, et al., Effects of microstructure of Ni barrier on bonding interface diffusion behaviors of Bi–Te-based thermoelectric material, J. Alloy. Compd. 817 (2020) 152731.

[15] F.A. Leavitt, J.C. Bass, N.B. Elsner, Thermolelectric Modul. gapless eggcrate (US5875098A) (1999).

[16] R.P. Gupta, K. Xiong, J.B. White, K. Cho, et al., Improvement in contact resistivity to thin film Bi2Te3. Thermoelectric materials 2010 - growth, properties, Nov. Charact. Methods Appl. (2010) 1267.

[17] L. Chen, F. Li, X. Hu, S. Bai, et al., A Bi2Te3-Based Thermoelectr. Gener. Device Fabr. Method (CN201110295849. 2) (2011) 13.

[18] F. Li, X.Y. Huang, W. Jiang, L.D. Chen, Interface microstructure and performance of Sb contacts in bismuth telluride-based thermoelectric elements, J. Electron. Mater. 42 (6) (2013) 1219–1224.

[19] R. Zybala, K. Kaszyca, M. Schmidt, M. Chmielewski, The properties of Bi2Te3-Cu joints obtained by SPS/FAST method, J. Electron. Mater. 48 (6) (2019) 3859–3865.

[20] L. Shen, Y. Chen, B. Niu, Z. Liu, et al., Optimization of interface materials between Bi2Te3-based films and Cu electrodes enables a high performance thin-film thermoelectric cooler, Acs Appl. Mater. Interfaces 14 (18) (2022) 21106–21115.

[21] S. El Oualid, F. Kosior, A. Dauscher, C. Candolfi, et al., Innovative design of bismuth-telluride-based thermoelectric micro-generators with high output power, Energy Environ. Sci. 13 (10) (2020) 3579–3591.

[22] D. Kraemer, J. Sui, K. McEnaney, H. Zhao, et al., High thermoelectric conversion efficiency of MgAgSb-based material with hot-pressed contacts, Energy Environ. Sci. 8 (4) (2015) 1299–1308.

[23] P. Kao, P. Shih, C. Dai, M. Liu, Fabrication and characterization of CMOS-MEMS thermoelectric micro generators, Sensors 10 (2) (2010) 1315–1325.

[24] W.P. Lin, D.E. Wesolowski, C.C. Lee, Barrier/bonding layers on bismuth telluride (Bi2Te3) for high temperature thermoelectric modules, J. Mater. Sci. Mater. Electron. 22 (9) (2011) 1313–1320.

[25] J.B. R, J.R. S, Development of a burst voltage measurement system for high-resolution contact resistance tests of thermoelectric heterojunctions, Eighteen-.-. Int. Conf. Thermoelectr. Proc. (1999) 249–251.

[26] C. Liao, C. Lee, W. Chen, Effect of interfacial compound formation on contact resistivity of soldered junctions between bismuth telluride-based thermoelements and copper, Electrochem. Solid-State Lett. 10 (9) (2007) P23.

[27] Z. Ren, Y. Lan, Q. Zhang, Adv. Thermoelectr.: Mater., Contacts, Devices, Syst. (2017).

[28] X.D. Zhu, L.L. Cao, W. Zhu, Y. Deng, Enhanced interfacial adhesion and thermal stability in Bismuth telluride/nickel/copper multilayer films with low electrical contact resistance, Adv. Mater. Interfaces 5 (23) (2018).

[29] L.Q. Chen, D.Q. Mei, Y.C. Wang, Y. Li, Ni barrier in Bi2Te3-based thermoelectric modules for reduced contact resistance and enhanced power generation properties, J. Alloy. Compd. 796 (2019) 314–320.

[30] B.H. Zhang, W. Zhu, L.L. Cao, Y.D. Yu, et al., Toward reduced interface contact resistance: controllable surface energy of Sb2Te3 films via tuning the crystallization and orientation, Acs Appl. Mater. Interfaces 14 (8) (2022) 10955–10965.

[31] C.D. Spataru, Y. He, F. Leonard, Atomistic study of an ideal metal/thermoelectric contact: the full-Heusler/half-Heusler interface, Apl. Mater. 7 (1) (2019).

[32] Y. Kim, Y. Jin, G. Yoon, I. Chung, et al., Electrical characteristics and detailed interfacial structures of Ag/Ni metallization on polycrystalline thermoelectric SnSe, J. Mater. Sci. Technol. 35 (5) (2019) 711–718.

[33] J. Shen, Z. Wang, J. Chu, S. Bai, et al., Low contact resistivity and interfacial behavior of p-type NbFeSb/Mo Thermoelectric junction, Acs Appl. Mater. Interfaces 11 (15) (2019) 14182–14190.

[34] P.H. Ngan, N. Van Nong, L.T. Hung, B. Balke, et al., On the challenges of reducing contact resistances in thermoelectric generators based on half-Heusler alloys, J. Electron. Mater. 45 (1) (2016) 594–601.

[35] W. Liu, H. Wang, L. Wang, X. Wang, et al., Understanding of the contact of nanostructured thermoelectric n-type Bi 2 Te 2.7 Se 0.3 legs for power generation applications, J. Mater. Chem. A 1 (42) (2013) 13093–13100.

[36] D. Zhao, H. Geng, X. Teng, Fabrication and reliability evaluation of CoSb3/W–Cu thermoelectric element, J. Alloy. Compd. 517 (2012) 198–203.

[37] N. Nandihalli, A short account of thermoelectric film characterization techniques, Mater. Today Phys. 36 (2023) 101173.

[38] S. Kianwimol, R. Sakdanuphab, N. Chanlek, A. Harnwunggmoung, et al., Effect of annealing temperature on thermoelectric properties of bismuth telluride thick film deposited by DC magnetron sputtering, Surf. Coat. Technol. 393 (2020) 125808.

[39] H. Kim, K. Kim, W.C. Choi, J. Kim, et al., Growth and thermoelectric properties of multilayer thin film of Bismuth telluride and indium selenide via rf magnetron sputtering, J. Nanosci. Nanotechnol. 12 (4) (2012) 3629–3632.

[40] Y. Zhang, Z. Qiao, X. Chen, Microwave-assisted elemental direct reaction route to nanocrystalline copper chalcogenides CuSe and Cu2Te, J. Mater. Chem. 12 (9) (2002) 2747–2748.

[41] C. Chotia, G.S. Okram, B. Mukherjee, Characterization and thermoelectric properties of polyol method-synthesized (Cu 7 Te 4) 1- x (Ag 2 Te) x (x =0, 0.03) nanocomposites, J. Mater. Sci. -Mater. Electron 31 (23) (2020) 20964–20971.

[42] M. Zhang, H. Park, J. Kim, H. Park, et al., Thermoelectric properties of ultralong silver telluride hollow nanofibers, Chem. Mat. 27 (15) (2015) 5189–5197.